Supporting Information

Table S1. X-ray crystal structures for dimeric $[(R_3P)Pd(Ar)X]_2$ complexes reported in the CCDC database (excluding cyclometalated complexes).

CCDC code	PR_3	Ar	X	*Config.*	ref
BIGFAA	P(neopentyl)$_3$	4-(*t*-Bu)-C_6H_4	Br	*anti*	[1]
BIFFII	P(neopentyl)$_3$	*o*-tolyl	Br	*anti*	[1]
CEMKEL	P(*m*-tolyl)$_3$	Ph	I	*anti*	[2]
CIXQUX	PMe_2Ph	*p*-tolyl	Cl	*anti*	[3]
EDULAS	PPh_3	2-Ph-C_6H_4	I	*anti*	[4]
ELENIS	P(*o*-tolyl)$_3$	2,4,6-$(CF_3)_3$-C_6H_2	Br	*anti*	[5]
GECWAN	PCy_2(Fc*)[a]	C_6F_5	I	*anti*	[6]
GECWOB	PCy_2(Fc*)[a]	C_6F_5	I	*anti*	[6]
GIDJAG	PCy_2[(2-Naphthyl)$_2$O]	4-CF_3-C_6H_4	Br	*anti*	[7]
HANXAX	PCy_2(2'-Me_2N-2-biphenyl) (DavePhos)	2-F-C_6H_4	Br	*anti*	[8]
JIMMEY	SPhos	Ph	Cl	*syn*	[9]
KONMIJ	PCy_3	(η^6-Ph)$Cr(CO)_3$	Cl	*anti*	[10]
LALXJH	PPh_3	2-Ar-4-arylidene-oxazolone	Br	*anti*	[11]
NAPDIT	Phosphabarrelene derivative	4-CN-C_6H_4	Br	*anti*	[12]
PAJGIS	PPh_2Me	Ph	Cl	*anti*	[13]
PAJGOY	PEt_3	*p*-tolyl	Cl	*anti*	[13]
POBVEH	P(o-tolyl)$_3$	6-Pr-C_6H_4	Br	*anti*	[14]
QEZPIU	PPh_3	Ph	I	*anti*	[15]
QWKAJ	P(1-Ad)$_2$Pr	4-CF_3-C_6H_4	Br	*anti*	[16]
TIPWEV	P(*o*-tolyl)$_3$	4-NO_2-C_6H_4	F	*syn*	[17]
TIPWIZ	P(*o*-tolyl)$_3$	Ph	F	*syn*	[17]
TIPWOF	P(*o*-tolyl)$_3$	*o*-tolyl	F	*syn*	[17]
TIPWUL	P(*o*-tolyl)$_3$	4-MeO-C_6H_4	F	*syn*	[17]
UHUZIH	PCy(*t*-Bu)$_2$	Ph	Br	*syn*	[18]
UHUZON	P(1-Ad)(*t*-Bu)$_2$	Ph	Cl	*syn*	[18]
UHUZUT	P(*t*-Bu)$_3$	2-CF_3-C_6H_4	Cl	*anti*	[18]

VACGEM	P(*i*-Pr)$_3$	Ph	F	*anti*	[19]
VACGIQ	PCy$_3$	Ph	F	*anti*	[19]
WIBSEG	P(*t*-Bu)$_3$	4-NO$_2$-C$_6$H$_4$	F	*syn*	[20]
YERNOZ	PPh$_3$	4-PPh$_3^+$-C$_6$H$_4$	I	*anti*	[21]
YORHET	PPr(*t*-Bu)$_2$	2-CF$_3$-C$_6$H$_4$	Br	*anti*	[22]

[a]Fc* = ferrocenyl derivative.

1. Preparation of dimer complex 1a (modified procedure)[23]

SPhos (399 mg, 0.97 mmole) and (TMEDA)PdMe$_2$ (264 mg, 1.04 mmole, 1.07 equiv) were added to a dry Schlenk tube, which was then evacuated and back filled with nitrogen. Chlorobenzene (8 ml) which had been previously stored over activated 4 Å MS for 1 week and degassed (purge-refill, N_2) was added to the tube under a flow of nitrogen. The mixture was stirred for 10 min at room temperature, before it was heated at 65 ºC for 7.5 hours.

The tube was removed from the oil bath and the solvent removed under reduced pressure. The residue was suspended in dry, degassed (purge-refill, N_2) toluene (24 ml), poured into a plastic centrifuge tube and stored in the freezer (–18 ºC) overnight. After centrifugation* (~2500 rpm for 15 min) the solution was transferred by cannula under N_2 to a clean plastic centrifuge tube and the solvent removed under reduced pressure. The residue was dissolved in $CHCl_3$ (9 mL), and pentane (1 mL) was added. The solution was stored in the freezer over the weekend resulting in precipitation of a yellow solid.
(* The precipitate is mainly [(TMEDA)Pd(Ph)Cl] with some SPhos and trace impurities.)
Centrifugation (~2500 rpm for 15 min) and decanting of the supernatant liquid gave a yellow solid residue, which was suspended in pentane (5 ml) and sonicated for 15 min. After cooling in a freezer overnight, the pale yellow solid was isolated by centrifugation and dried under vacuum. The decanted supernatant ($CHCl_3$/pentane) was concentrated to approx. half volume under reduced pressure and additional pentane added (1 mL). A further crop of solid was obtained by repeating the purification procedure outlined above.
Total product obtained: 290 mg, 47%
This procedure was replicated a few times during the course of this study. Typical yields range from 35%–55%, additional product can be recovered by combining and recycling the supernatant.

2. EXAFS spectroscopy

As stated in the main paper the Pd K-edge EXAFS data was reduced using PAXAS[24] and then analysed using full curved wave scattering theory using EXCURV.[25]

Figure S1 shows how the different scattering elements contribute to the fitting of the k^3-weighted spectrum of the solid SPhos complex.

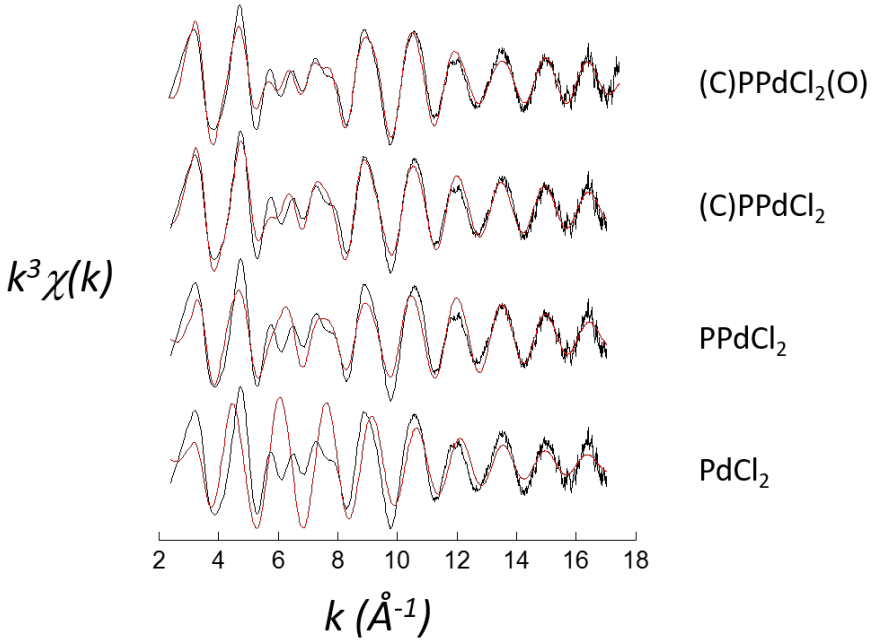

Figure S1. Stepwise fitting of the Pd K-edge EXAFS derived from the solid SPhos complex.

We note firstly that most of the EXAFS envelope can be very well described without explicitly adding the Pd-Pd scattering interaction that exists at ca 3.29 Å. In the table given below it is included but the high levels of disorder associated with this interaction mean that even in the solid state this scattering interaction is not statistically significant to the fit; the same is true of the Pd-O contribution arising from the phosphine ligand and apical to the square planar arrangement of the remaining scatterers.

What can be determined from this stepwise fitting is that it is the combined, and to some degrees destructive, interference between the Cl, P and C atoms within a square planar geometry that dominate the EXAFS envelope in the range $4.5 < k < 8.5$: it is only when the square planar geometry around the Pd is completed that this region is well fitted by the analysis and become deterministic of the dominance of monomers or dimers in solution (see below).

Supporting Information

Figure S2 shows the result of an equivalent stepwise addition of scatterers to the spectrum derived from SPhos dissolved in DMF.

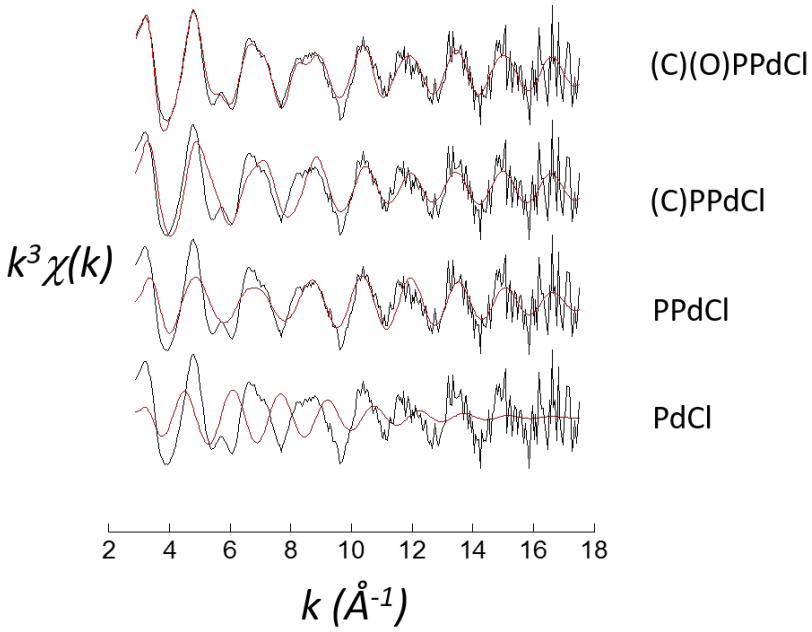

Figure S2. Stepwise fitting of a monomeric model to the Pd K-edge EXAFS derived from the solid SPhos complex dissolved in DMF.

In this case it is readily observable that the structure of the EXAFS in the 4.5 < k < 8.5 range is radically different to that observed from the dimeric solid. Stepwise fitting again shows that a good fit to this data is only achieved upon the completion of a square planar geometry that only contains a single Pd-Cl interaction, but that contains a new Pd-O contribution at a distance (see below) consistent with it arising from an interaction with the solvent. Ergo in DMF and at the concentrations used the Pd complex is found in a momomeric form.

However, a reasonable question to ask, given that we are unable to directly observe the PdPd scattering in the solid state dimer, is whether we can obtain a fit to the DMF data using a dimeric model of the complex?

Figure S3 shows that such a fitting can be achieved.

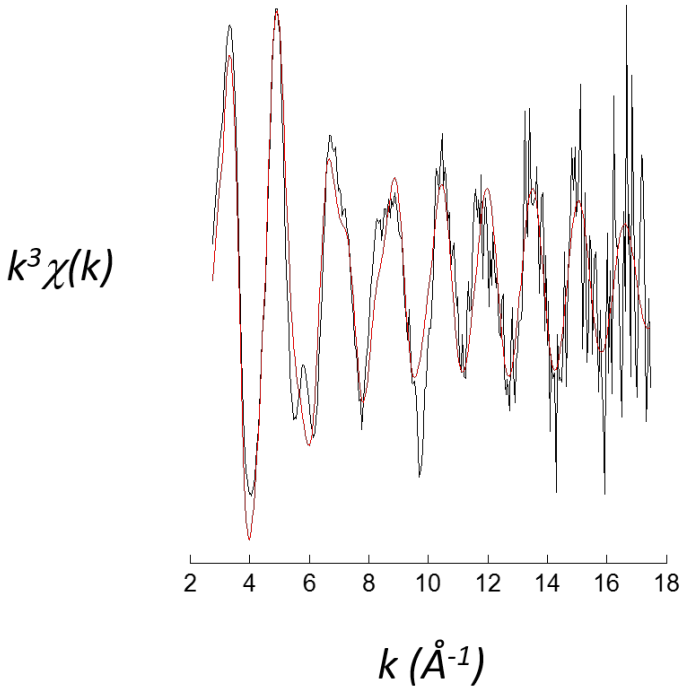

Figure S3. An achievable fit to the Pd K-edge EXAFS derived from the SPhos complex dissolved in DMF, as a dimer.

Whilst this fit appears just as reasonable as that derived from a monomeric species, it comes with numerous problematic issues. To achieve this fit, and to match the required convolution of scattering between Pd-P and Pd-Cl contributions, one of the Cl atoms of the notional dimer has a radically reduced bond length (2.26 Å rather than 2.42 Å), and a much higher disorder parameter (0.023). The end result is a physically unreasonably and highly asymmetrically bonded dimer. Therefore, though a fit to a dimer can be achieved for the spectrum collected in DMF, it is categorically rejected in favour of the structurally reasonable monomer that is then concluded to be the majority species present in this solvent.

Table S2. EXAFS fitting data

	Solid		Toluene		Dioxane		DMF	
k range	k_{min} = 2.0	k_{max} = 17.5	k_{min} = 2.0	k_{max} = 17.5	k_{min} = 2.0	k_{max} = 17.5	k_{min} = 2.0	k_{max} = 17.0
E_F	–7.63		–6.231		–7.55		–6.994	
R%	32.3		38.0		58.8		42.8	
Atom	R (Å)	DW ($2\sigma^2$)	R (Å)	DW ($2\sigma^2$)	R (Å)	DW ($2\sigma^2$)	R (Å)	DW ($2\sigma^2$)

Cl	2.37	0.012	2.40	0.009	2.40	0.011	2.42	0.015
Cl	2.45	0.006	2.46	0.011	2.45	0.012		
P	2.24	0.009	2.25	0.006	2.25	0.006	2.24	0.007
C	2.01	0.009	2.00	0.006	1.99	0.006	1.98	0.006
O	2.94	0.006	2.93	0.007	2.94	0.009	2.11	0.010
Pd	3.29	0.03	3.25	0.032	3.24	0.035		

E_F = the edge position relative to the vacuum zero (Fermi energy)

R% = 33.37 = ($\int |\chi^T - \chi^E|k^3dk/|\chi^E|k^3dk$) x 100% where χ^T and χ^E are the theoretical and experimental EXAFS and k is the photoelectron wave vector; the Debye–Waller factor = $2\sigma^2$, where σ is the root mean square internuclear separation.

AFAC, related to the proportion of electrons performing an EXAFS type scatter on absorption, is 0.875.

We note that, though included for completeness, the long O and Pd scattering interactions are never found to be statistically significant to the fits of the EXAFS data. As described above it is only contributions from the immediate square planar coordination surrounding the Pd atoms that are significant and can be used to determine whether the SPhos complex remains as a dimer or a monomer in solution.

3. NMR spectroscopy

DOSY experiments were measured at a temperature of 298 K on a Bruker 500 MHz AVANCE III HD spectrometer running TopSpin3.2 and equipped with a z-gradient bbfo/5mm tuneable SmartProbe and a GRASP II gradient spectroscopy accessory providing a maximum gradient output of 53.5 G/cm. The ^{1}H DOSY spectra were collected using the Bruker pulse program ledbpgp2s at a frequency of 500.13 MHz with a spectral width of 5000 Hz (centred on 4 ppm) and 32768 data points. A relaxation delay of 10 s was employed along with a diffusion time (Δ) of 40 ms and a longitudinal eddy current delay (LED) of 5 ms. Bipolar gradients pulses ($\delta/2$) of 2.2 ms and homospoil gradient pulses of 1.1 ms were used. The gradient strengths of the 2 homospoil pulses were –17.13% and –13.17%. 16 experiments were collected with the bipolar gradient strength, initially at 2% (1st experiment), linearly increased to 95% (16th experiment). All gradient pulses were smoothed-square shaped (SMSQ10.100) and after each application a recovery delay of 200 μs was used. The data was processed using 16384 data points in the direct dimension applying an exponential function with a line broadening of 1 Hz and 128 data points in the indirect dimension. Further processing and calculation of the diffusion constants were performed using the MestreNova software package (version 7.0.2).

Supporting Information

Diffusion constants were calculated using the Bayesian DOSY transform algorithm[26] included with the MestreNova software package:

$$S(f,z) = S_A(f)\exp(-D_A Z)$$

$$Z = \gamma^2 G^2 \delta^2 (\Delta - \delta/3)$$

Stokes-Einstein equation:

$$D = \frac{k_B T}{8\pi\eta r}$$

$$\frac{r_{C_7D_8}}{r_{CDCl_3}} = \frac{D_{CDCl_3} \times \eta_{CDCl_3}}{D_{C_7D_8} \times \eta_{C_7D_8}}$$

r = molecular radius (assumes molecule is spherical)

η = viscosity

D = diffusion constant

The viscosity coefficients of the deuterated solvents used here are those reported by Morris:[27]

η_{CDCl_3} = 5.28 g·m^{-1}·s^{-1} and $\eta_{C_7D_8}$ = 5.39 g·m^{-1}·s^{-1}.

	Bayesian		deuterio 25 ºC		deuterio 25 ºC
	D_H	D_P	η		D × η
$CDCl_3$	2.03E-05	2.02E-05	0.528	×10^{-3} kg·m^{-1}·s^{-1}	1.07E-05
toluene	6.31E-06		0.539	×10^{-3} kg·m^{-1}·s^{-1}	3.40E-06

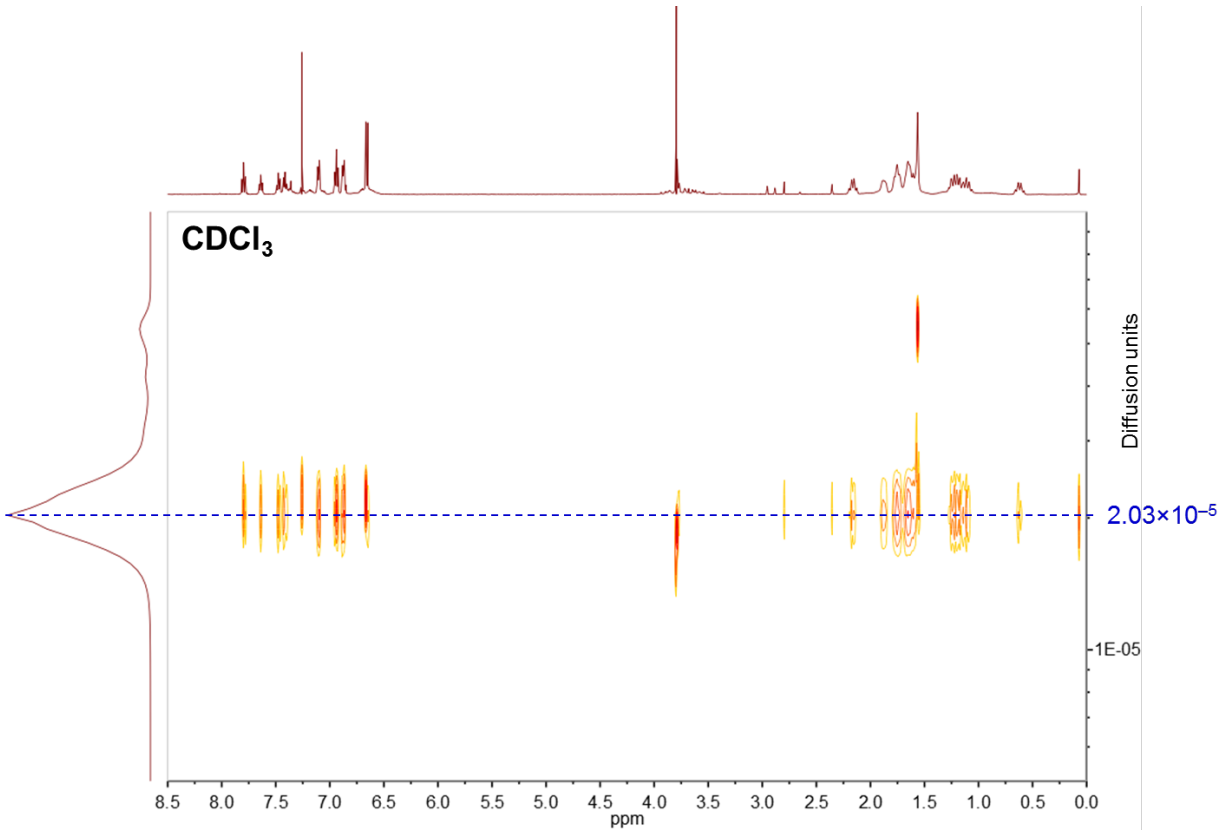

Figure S4. DOSY spectrum of complex **1a** in $CDCl_3$.

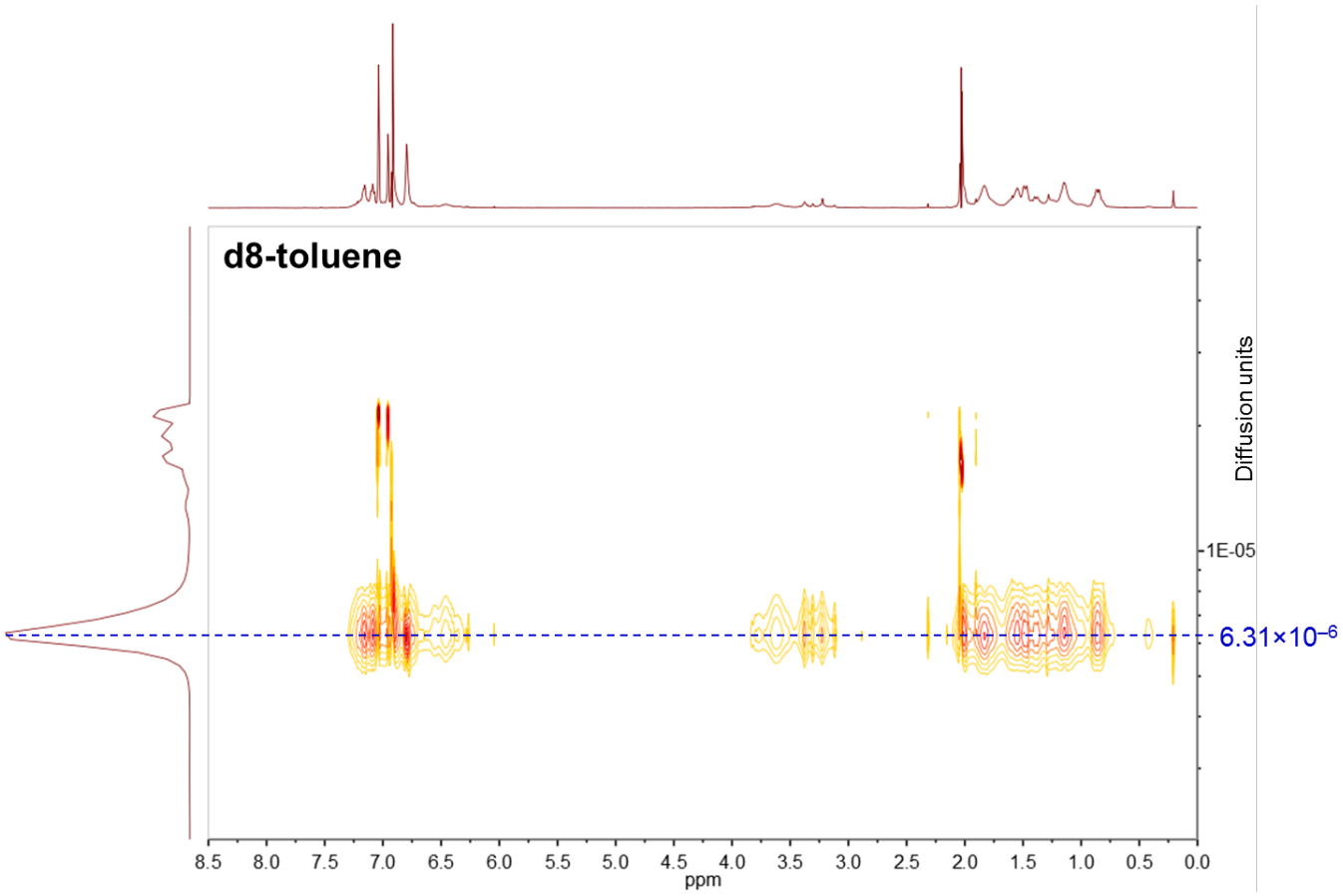

Figure S5. DOSY spectrum of complex **1a** in toluene-d_8.

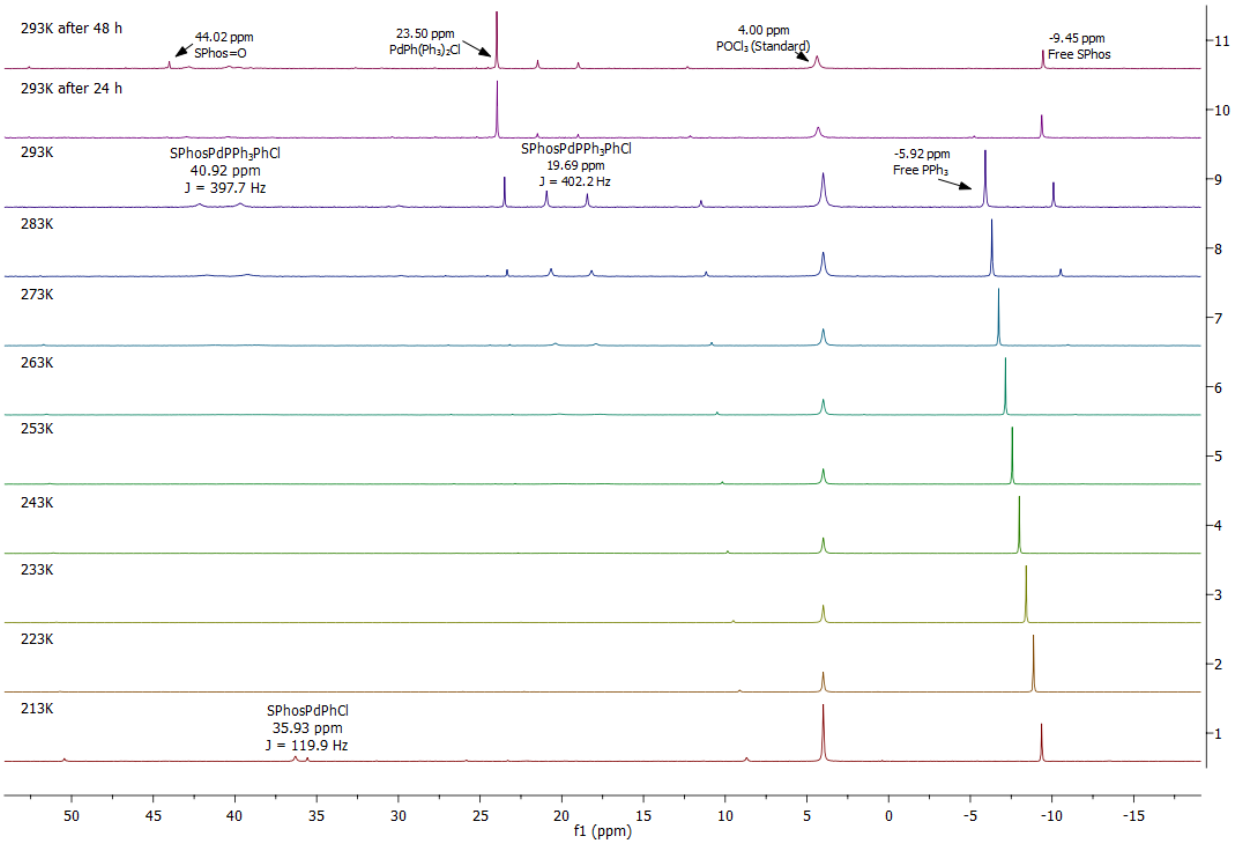

Figure S6. VT NMR of a mixture of complex **1a** and PPh_3 in toluene-d_8.

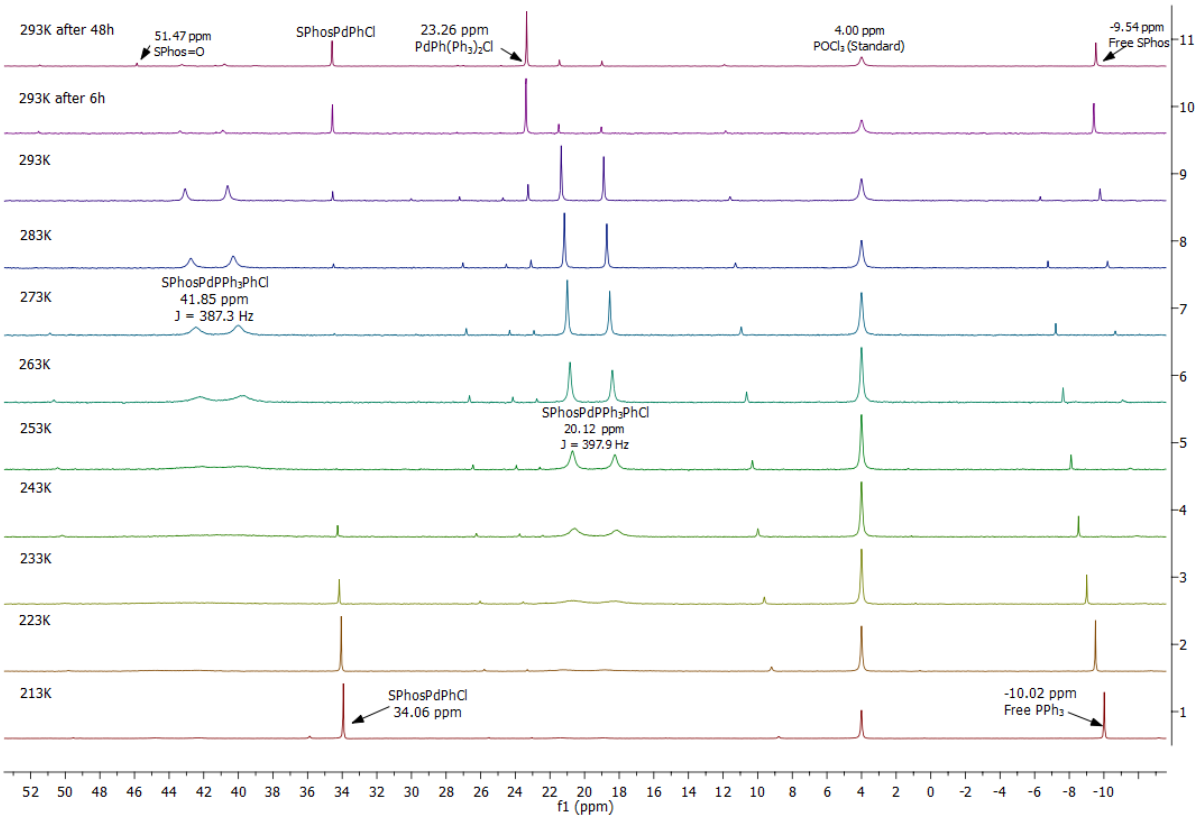

Figure S7. VT NMR of a mixture of complex **1a** and PPh_3 in CD_2Cl_2.

4. Mass Spectrometry

Mass spectrometry was performed at Imperial College London using a Waters LCT Premier (ES-ToF)/Acquity i-Class spectrometer, operating in ES+ mode, using 2 kV capillary voltage and 30 V sample cone voltage. Samples of complex **1a** were dissolved in either DMF or toluene prior to injection into the spectrometer.

(i) Complex **1a** in DMF: In DMF, the most significant peaks in the mass spectrum can be assigned to the monomeric form of the complex with the loss of chlorine [SPhosPd(Ph)] (591–598) and its monosolvate [SPhosPd(Ph)dmf] (664–673). The monosolvate of the intact monomer is only observed as a complex with Li^+ (702–710) or Na^+ (722–730). Signals due to the Na adduct of dimeric complex **1** (1276–1288) and the dimer with the loss of Cl (1218–1230) are observed, but are weak compared with those due to the monomeric form.

(ii)

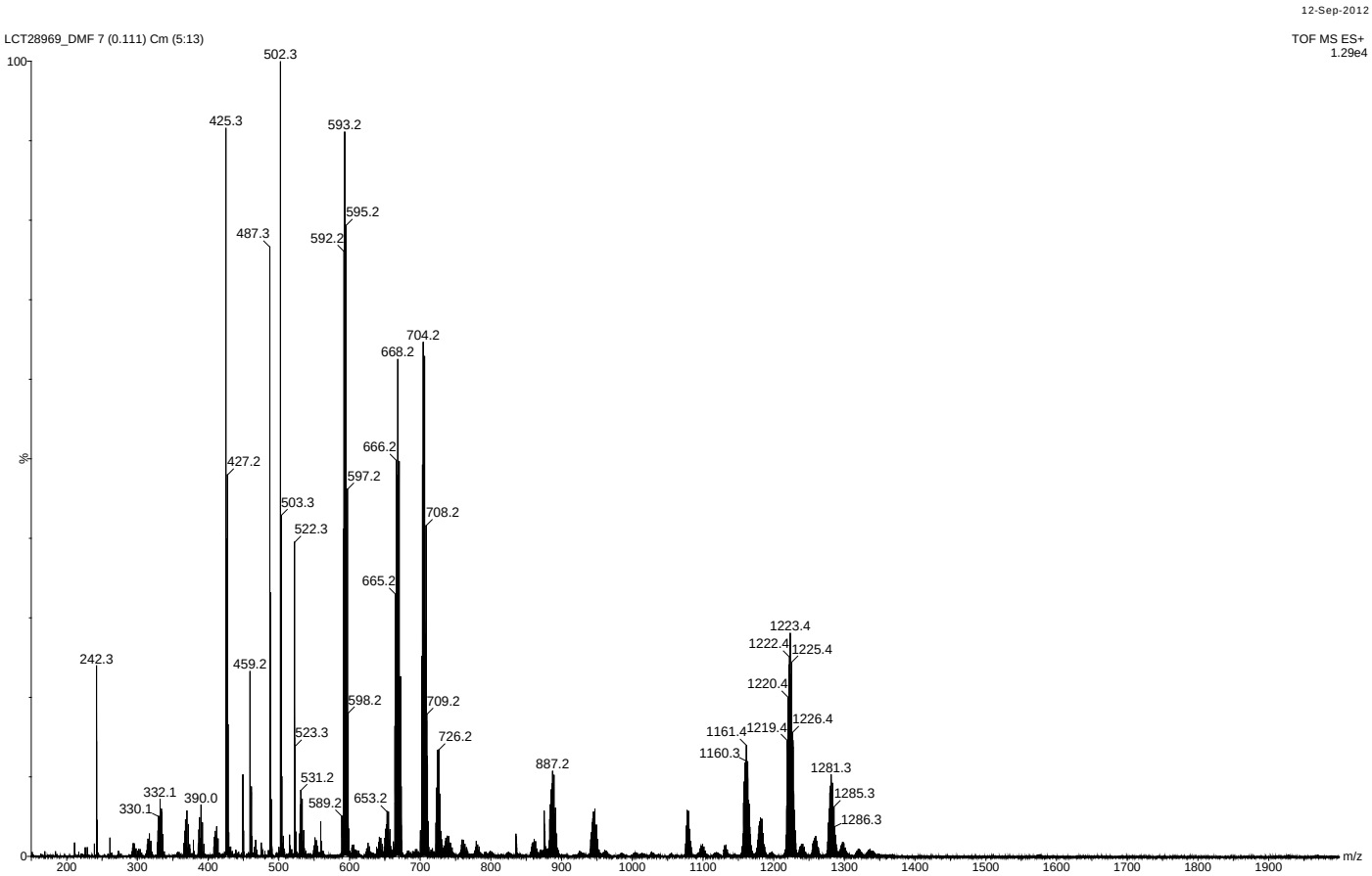

(iii) Complex **1a** in toluene: the mass spectrum of the toluene solution shows high molecular weight species to be more abundant including the dimer with loss of Cl (1218–1230). Although not all observed masses could be readily assigned, the formation of higher mass species in the toluene solution, close to that of the dimer, support our previous data showing that the main complex in solution is likely to be the dimeric form.

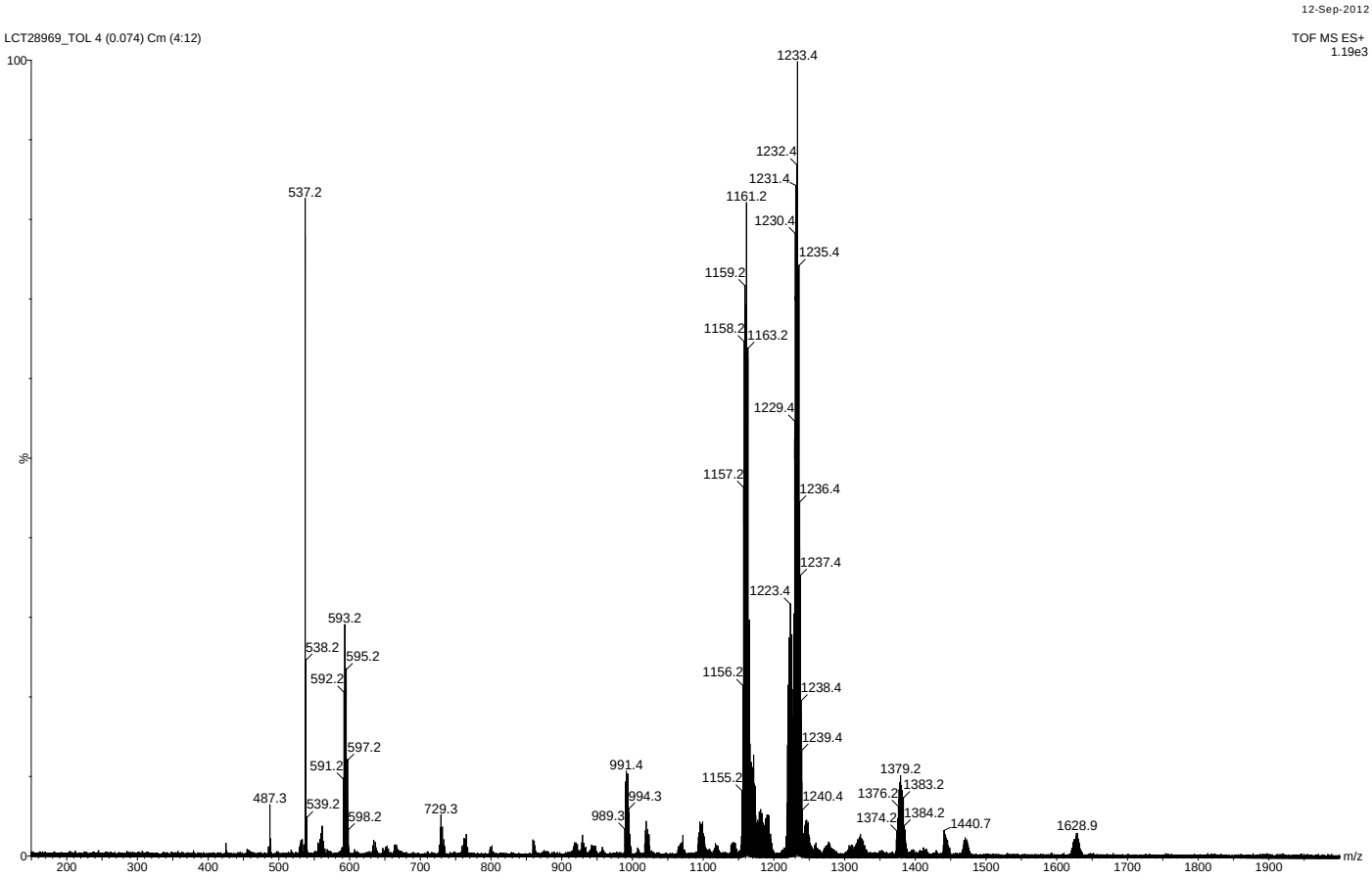

Supporting Information

Isotope distribution patterns:

(iii) $[SPhosPd(Ph)]^+$ (591–598)

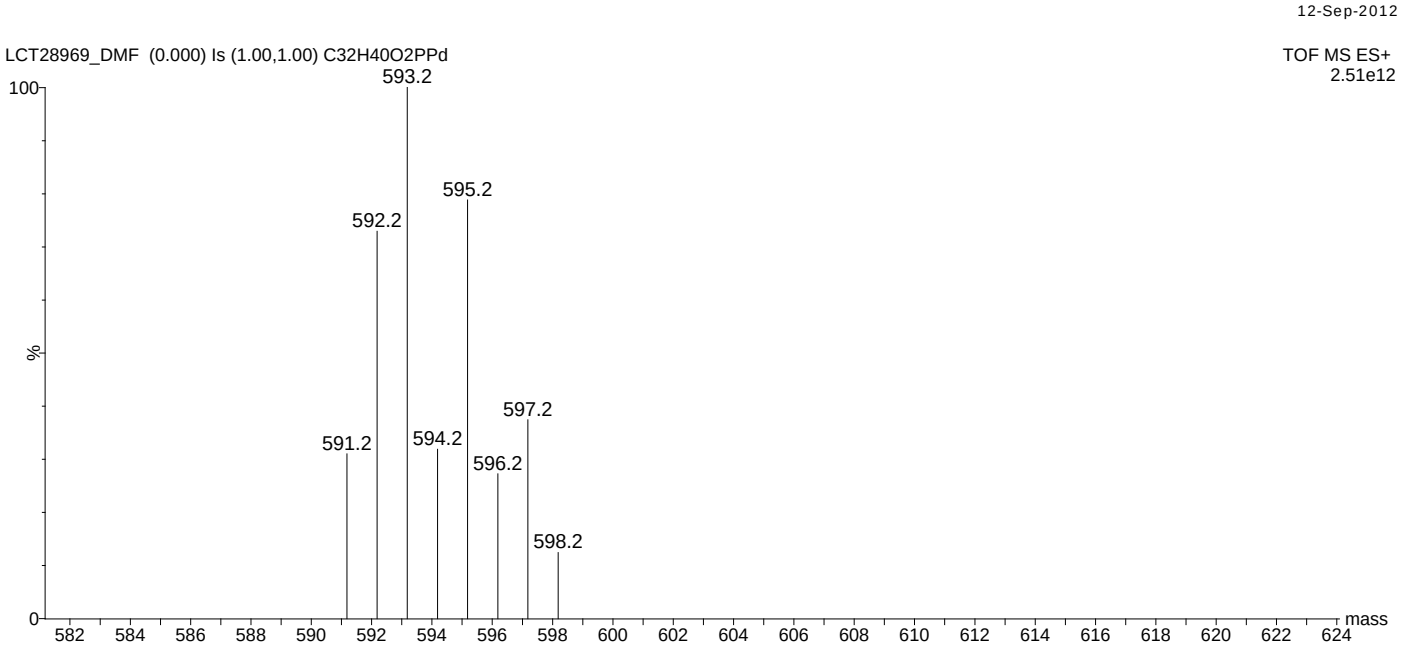

(iv) Monosolvate [SPhosPd(Ph)(DMF)], observed as a Li^+ (702–710) complex.

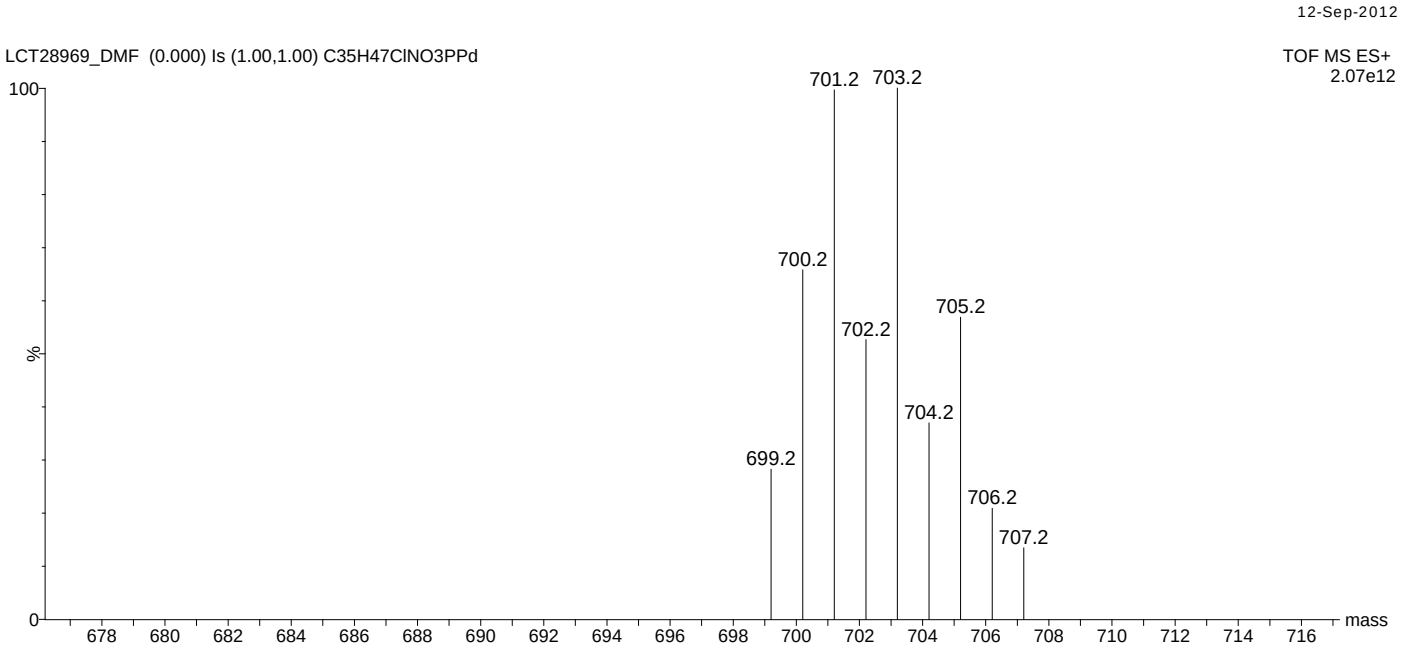

(v) Dimer [**1a**- Cl]$^+$

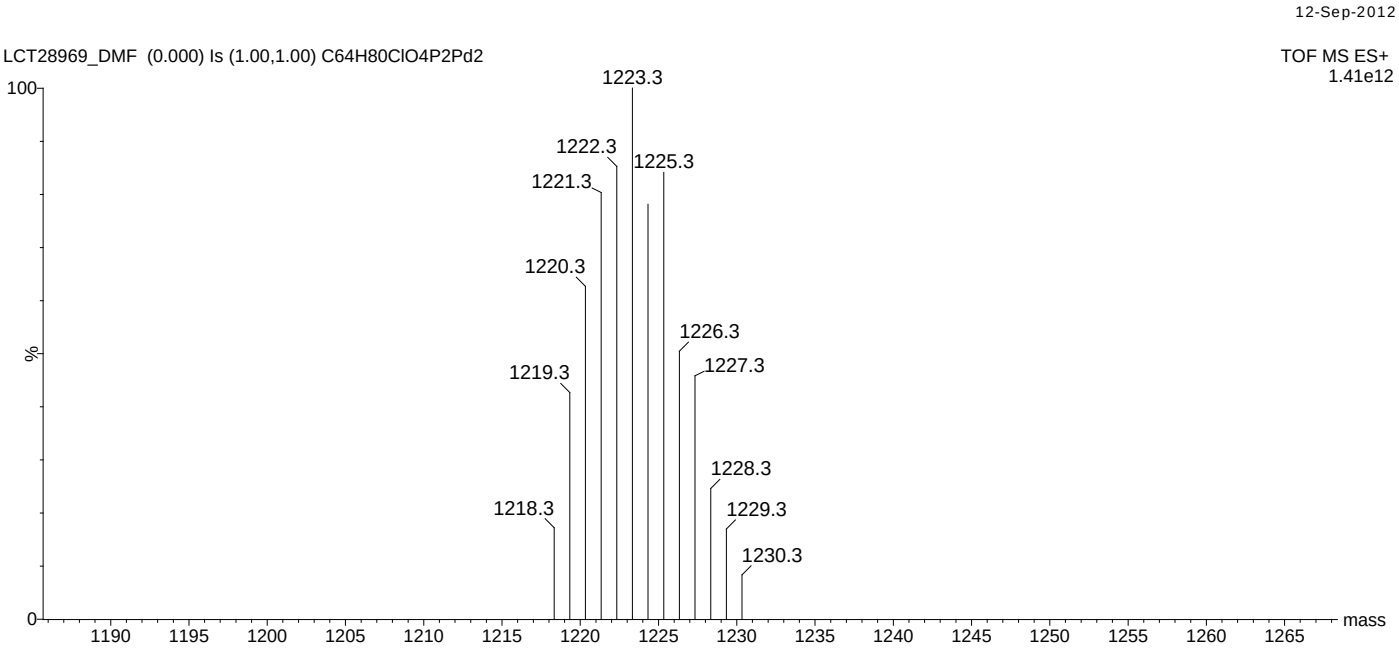

5. DFT calculations

Three density functionals were assessed: hybrid functionals WB97XD and M06L take dispersion into account, while the 'standard' density functional B3LYP only approximates short-range correlation effects. For Pd, the 6-31G** basis set was extended using Def2TZVP, which was developed by the Ahlrichs group and previously found to afford the best fit for organometallic compounds.[28] The outputs from all three calculations were compared to experimental data afforded by X-ray crystallography (Table S3). While very accurate prediction of the Pd-Ph bond length can be obtained, the Pd-Cl and Pd-P distances were generally overestimated by ≥1.2%, although the correct relative ordering was observed, *i.e.* the Pd-Cl *trans* to P is shorter than the corresponded Pd-Cl *trans* to C, as expected due to the σ-donor exerting a greater *trans*-effect than the π-acceptor.

Table S3. Experimental bond lengths (Å) vs calculated values for complex *syn*-**1a**. Deviation from experimental values indicated in ***red bold italics***.

	Pd-Cl (Å)	Pd-P (Å)	Pd-C (Å)
Experimental[a]	2.41 (*trans* to P)	2.26	2.00
	2.43 (*trans* to C)		
B3LYP/Def2TZVP	2.47 (*trans* to P), ***+0.06***	2.32, ***+0.06***	2.00
	2.53 (*trans* to C), ***+0.10***		
WB97xd/Def2TZVP	2.44 (*trans* to P), ***+0.03***	2.28, ***+0.02***	2.00

	2.47 (*trans* to C), ***+0.04***		
M06L/Def2TZVP	2.51 (*trans* to P), ***+0.10***	2.28, ***+0.02***	2.00
	2.53 (*trans* to C), ***+0.10***		

[a]Values obtained from crystallographic data reported for JIMMEY.

Outputs from these calculations have been deposited on an open-access server, which may be accessed via the following links:

syn-**1a** (gas phase): http://hdl.handle.net/10042/199296

anti-**1a** (gas phase): http://hdl.handle.net/10042/196213

syn-**1a** (toluene): http://hdl.handle.net/10042/199295

anti-**1a** (toluene): http://hdl.handle.net/10042/199294

syn-**1a** (DMF): http://hdl.handle.net/10042/199293

anti-**1a** (DMF): http://hdl.handle.net/10042/196225

cis- & *trans*-**2a** (toluene): http://hdl.handle.net/10042/199299

cis- & *trans*-**2a** (DMF): http://hdl.handle.net/10042/199298

2 x *cis*-**2a** (toluene): http://hdl.handle.net/10042/199300

2 x *cis*-**2a** (DMF): http://hdl.handle.net/10042/199297

References

1. S. M. Raders, J. N. Moore, J. K. Parks, A. D. Miller, T. M. Leißing, S. P. Kelley, R. D. Rogers and K. H. Shaughnessy, *J. Org. Chem.*, 2013, **78**, 4649-4664.
2. W. Zawartka, A. M. Trzeciak, J. J. Ziółkowski, T. Lis, Z. Ciunik and J. Pernak, *Adv. Synth. Catal.*, 2006, **348**, 1689-1698.
3. K. R. Chaudhari, A. P. Wadawale, M. Kumar and V. K. Jain, *J. Organometallic Chem.*, 2014, **760**, 55-59.
4. S. Brown and G. Crundwell, *Acta Cryst. Section E*, 2012, **68**, m1526.
5. C. Bartolomé, P. Espinet, Jose M. Martín-Alvarez and F. Villafañe, *Eur. J. Inorg. Chem.*, 2003, **2003**, 3127-3138.
6. S. Teo, Z. Weng and T. S. A. Hor, *Organometallics*, 2006, **25**, 1199-1205.
7. Z. Huang, L. H. Lim, Z. Chen, Y. Li, F. Zhou, H. Su and J. Zhou, *Angew. Chem. Int. Ed.*, 2013, **52**, 4906-4911.
8. P. Larini, C. E. Kefalidis, R. Jazzar, A. Renaudat, E. Clot and O. Baudoin, *Chem. Eur. J.*, 2012, **18**, 1932-1944.
9. M. R. Biscoe, T. E. Barder and S. L. Buchwald, *Angew. Chem. Int. Ed.*, 2007, **46**, 7232-7235.

10. V. Dufaud, J. Thivolle-Cazat, J. M. Basset, R. Mathieu, J. Jaud and J. Waissermann, *Organometallics*, 1991, **10**, 4005-4015.
11. G.-D. Roiban, E. Serrano, T. Soler, M. Contel, I. Grosu, C. Cativiela and E. P. Urriolabeitia, *Organometallics*, 2010, **29**, 1428-1435.
12. P. Ribagnac, M. Blug, J. Villa-Uribe, X.-F. Le Goff, C. Gosmini and N. Mézailles, *Chem. Eur. J.*, 2011, **17**, 14389-14393.
13. K. R. Chaudhari, A. P. Wadawale and V. K. Jain, *J. Organometallic Chem.*, 2012, **698**, 15-21.
14. F. Paul, J. Patt and J. F. Hartwig, *J. Am. Chem. Soc.*, 1994, **116**, 5969-5970.
15. W. J. Marshall, R. J. Young and V. V. Grushin, *Organometallics*, 2001, **20**, 523-533.
16. A. G. Sergeev, A. Zapf, A. Spannenberg and M. Beller, *Organometallics*, 2008, **27**, 297-300.
17. V. V. Grushin and W. J. Marshall, *Organometallics*, 2007, **26**, 4997-5002.
18. F. Barrios-Landeros, B. P. Carrow and J. F. Hartwig, *J. Am. Chem. Soc.*, 2009, **131**, 8141-8154.
19. V. V. Grushin and W. J. Marshall, *Angew. Chem. Int. Ed.*, 2002, **41**, 4476-4479.
20. D. V. Yandulov and N. T. Tran, *J. Am. Chem. Soc.*, 2007, **129**, 1342-1358.
21. H. Lang, D. Taher, B. Walfort and H. Pritzkow, *J. Organometallic Chem.*, 2006, **691**, 3834-3845.
22. A. G. Sergeev, A. Spannenberg and M. Beller, *J. Am. Chem. Soc.*, 2008, **130**, 15549-15563.
23. T. E. Barder, M. R. Biscoe and S. L. Buchwald, *Organometallics*, 2007, **26**, 2183-2192.
24. N. Binsted, PAXAS: Programme for the analysis of X-ray absorption spectra, University of Southampton, 1988.
25. N. Binsted, EXCURV98 CCLRC Daresbury Laboratory computer program, 1998
26. C. Cobas and S. Sýkora; SMASH 2008 Conference, September 7–10, 2008, Santa Fe (NM), USA: http://mestrelab.com/pdf/posters/Poster_2008_BayDOSY.pdf.
27. R. Evans, Z. Deng, A. K. Rogerson, A. S. McLachlan, J. J. Richards, M. Nilsson, and G. A. Morris, *Angew. Chem. Int. Ed.*, 2013, **52**, 3199–3202.
28. K. Eichkorn, F. Weigend, O. Treutler and R. Ahlrichs, *Theor. Chem. Acc.*, **97**, 119-124.